Available online at www.sciencedirect.com
SCIENCE DIRECT
Polymer 46 (2005) 887–901
polymer
www.elsevier.com/locate/polymer

Microfibrillar composites based on polyamide/polyethylene blends. 1. Structure investigations in oriented and isotropic polyamide 6

Nadya Dencheva[a], Teresa Nunes[b], M. Jovita Oliveira[a], Zlatan Denchev[a,*]

[a]*Department of Polymer Engineering, IPC—Institute for Polymers and Composites, University of Minho, 4800-058 Guimarães, Portugal*
[b]*IST–Instituto Superior Técnico, Departamento de Engenharia de Materiais and ICTPOL/IST, Av. Rovisco Pais 1, Lisboa, 1049-001, Portugal*

Received 20 July 2004; received in revised form 10 November 2004; accepted 22 November 2004
Available online 19 December 2004

Abstract

The present paper discloses the structural changes caused by heating of polyamide 6 (PA6) samples with different thermal and mechanical histories in the 30–240 °C range. Wide and small-angle X-ray scattering (WAXS and SAXS) of synchrotron radiation, as well as solid-state nuclear magnetic resonance spectroscopy (NMR) measurements are performed. The NMR spectra show that in both isotropic and oriented samples there is a co-existence of α and γ-PA6 crystalline forms. Deconvolution of the WAXS patterns is performed to follow the temperature dependence of the unit cell parameters of the α and γ-forms and also of the equatorial (ECI) and total crystallinity indexes (CI), evaluating the contributions of the two crystalline phases. Estimates for the long spacing and for the average thicknesses of the crystalline (l_c) and amorphous (l_a) phases within the lamellae are calculated as a function of the heat treatment employing analysis of the linear correlation function calculated from the SAXS patterns. The X-ray results allowed the conclusion that upon heat treatment up to 160–200 °C, intensive transitions between the PA6 crystalline forms take place, whereby the content of the initial major crystalline phase decreases and that of the initial minor one increases reaching almost 1:1. Close to 200 °C a general trend toward increasing the content of the α-form is registered. The influence of annealing and quenching after melting on the PA6 crystalline structure is also studied.

Keywords: Synchrotron X-ray scattering; Solid state NMR; Polyamide 6

1. Introduction

Polyamides belong to the polymers most frequently used in engineering applications. To improve some of their shortcomings such as a certain fragility, high water absorption, insufficient impact strength, etc. polyamides are mixed with other polymers [1,2]. Among the large number of combinations studied, those based on high-density polyethylene (HDPE) and polyamide-6 (PA6) have been subject of particular attention. These blends are a typical example where the two components possess complimentary properties [3–6]. Polyolefin/polyamide systems show high impact strengths [4,7–9], excellent thermal, mechanical and oil resistance properties [10,11]. These blends are of big importance for applications in food packing due to the good oxygen barrier of the polyamide and the excellent moisture barrier of the polyolefin [12].

Most of the commercially available polymer blends are used as isotropic (non-oriented) materials. However, blending of two or more neat polymers may be combined with adequately chosen mechanical and thermal treatment. In such a way, in situ reinforced polymer–polymer composites can be obtained as indicated for the first time by Fakirov et al. [13–15]. Manufacturing of these composites includes three main processing steps: (i) melt-blending of the starting neat polymers and extrusion; (ii) cold-drawing of the blend, and (iii) thermal treatment of the oriented blend at $T_1 < T < T_2$ where T_1 is the melting temperature of the lower melting component and T_2 is that of the higher melting one. As a result, polymer blends are transformed into composite materials in which an isotropic polymer matrix is reinforced by highly oriented fibrils of another polymeric phase [16].

* Corresponding author. Tel.: +351 253 510 332; fax: +351 253 510 339.
E-mail address: denchev@dep.uminho.pt (Z. Denchev).

0032-3861/$ - see front matter © 2004 Elsevier Ltd. All rights reserved.
doi:10.1016/j.polymer.2004.11.105

Since the diameters of the reinforcing fibrils are generally in the range of 10^{-5}–10^{-6} m, these systems are also known as 'microfibrillar composites' (MFC).

The mechanical properties of the known MFC materials are quite promising [16,17]. On the one hand, as a rule, they exhibit Young's moduli and tensile strengths about 30–50% higher than the average value of the matrix components becoming comparable to those of the corresponding glass fiber reinforced systems. On the other hand, no mineral additives are used thus increasing the mechanical integrity of these materials and reducing the wear of the processing machines. The increasing need for recycling of mixed wastes is also an important prerequisite for further studies in the field of MFC materials.

Among the numerous polymer blends that are reportedly used for preparation of MFC, those consisting of a polyolefin matrix reinforced by either poly(ethylene terephthalate) [18–21] or polyamide [22,23] fibrils deserve special attention. These systems are potentially interesting for large-scale manufacturing since they are based on neat polymers of major production scale and importance and could open a new way in the recycling of polyolefin, polyester and polyamide wastes. The last investigations on the preparation and properties of PA6 and PA12-reinforced HDPE revealed that in order to optimize the mechanical properties of these MFC, an in-depth understanding is needed on the structure evolution in the reinforcing polyamide phase taking place during the orientation and isotropization stages.

There exist a number of studies on the structure development of isotropic and oriented PA6 samples at various processing conditions. It is well known that PA6 is a semicrystalline polymer characterized by two basic crystalline modifications designated as α and γ-phases. The α-phase is monoclinic, whereas the γ-phase is considered by some authors to have pseudo-orthorhombic [24,25] or pseudo-hexagonal lattice [26]. The α-crystalline form is organized as anti-parallel polymer chains wherein the amide groups and the CH_2 units lay within the same plane. H-bond formation occurs between adjacent anti-parallel chains, thus forming sheets of H-bonded chains. This structure with anti-parallel polymer chains can be realized in the presence of chain folding [27]. The γ-crystalline form of PA6 is built up of parallel polymer chains. To enable H-bond formation in this case, the amide linkages should twist by approximately 60° out of the plane of the molecular sheets, which explains the slightly smaller unit cell [26] and the inferior hydrogen bonding [27] in the γ-crystal as compared to those in the α-form.

The two crystalline forms of PA6 normally co-exist. Which one of them is predominant will depend, as repeatedly reported, on the sample preparation conditions: temperature of crystallization, external stress applied, presences of moisture or of certain additives [26]. Several investigations [28,29] showed that crystallization of PA6 for extended periods below 130 °C leads solely to formation of γ-crystallites, whereas annealing above 190 °C produces only the α-form. Temperatures in between these limits result in a mixture of the two forms, with higher fractions of α-form being produced at higher temperatures. The disappearance of the γ-form close to 190 °C in PA6 is commonly referred to as 'Brill transition' [30–34]. It is generally accepted that rapid cooling and low temperature crystallization promotes the γ-form of PA6, whereas higher crystallization temperatures or slow cooling results in α-crystalline modification [31,35–37].

Application of external stress can also result in phase transitions in PA6. As shown by Murthy et al. [38–40] by means of small-angle X-ray scattering (SAXS) and wide-angle X-ray scattering (WAXS) in a pre-drawn, relaxed PA6 fiber, α to γ-crystal transitions possibly occurs through a metastable intermediate crystalline phase. On the contrary, the results of Samon et al. [27] were more consistent with a γ to α-transition. These authors performed synchrotron SAXS and WAXS studies cold-drawing a PA6 fiber while irradiating. Rhee and White [41] studied biaxially oriented PA6 films and disclosed a third PA6 phase -β or pleated α-phase. According to these authors, this phase is not very stable and is easily transformed into the more stable α or γ-forms, whereas the γ-crystal cannot be transformed into other forms.

It may be concluded that there is still some debate on the structure of PA6 samples prepared under different processing conditions including heat treatment and deformation. It is not quite clear what changes occur in the PA6 microstructure upon orientation by cold drawing and subsequent annealing. As mentioned above, in the HDPE/PA6 microfibrillar composite the polyamide is the reinforcing phase. Therefore, it is important to study the structure development of PA6 under the concrete conditions of HDPE/PA6 composite formation.

In the present work we studied the morphological changes in oriented or isotropic PA6 samples with heat treatments below and above the melting point employing solid-state NMR and synchrotron WAXS and SAXS measurements. The paper is a part of a comprehensive study on HDPE/PA6 and HDPE/PA12 precursors and microfibrillar composites prepared thereof, which will be communicated in the next articles of this series.

2. Experimental part

2.1. Materials and samples preparation

Four different PA6 samples were investigated, all of them being prepared using as a starting material *Ultramid B 35* (BASF, Germany)—a medium-viscosity, general purpose polycaproamide grade with a melting temperature $T_m = 220$ °C (DSC) obtained by ring-opening polymerization.

The first sample designated as 'PA6 granules' comprises

as-supplied granules with no initial mechanical or heat treatment.

The second sample designated as 'PA6 film' was obtained by compression molding of dry PA6 granules for 5 min at 250 °C followed by cooling (ca. 20 deg/min) to room temperature.

The third sample was called 'oriented cable' and was prepared in an extruder line including a Leistritz LSM 30.34 intermeshing co-rotating twin-screw extruder, two water baths, two haul-off units and a winder positioned downstream. The extrusion was performed at a set temperature of 250 °C. The resulting extrudate was cooled in the first water bath down to 12 °C while drawing it at a draw ratio (DR) of $\lambda = 2.6$. The final drawing was performed in the second haul-off unit after heating the stretched cable up to 90–96 °C in the second water bath, whereby the total DR of the PA6 oriented cable reached values between 14 and 16. More details about the extruder line can be found elsewhere [22].

Some oriented PA6 cables were annealed with free ends at 120, 160 or 200 °C in a Mettler FP 82 hot stage and designated as 'annealed oriented cable', which was the fourth PA6 sample investigated. Each annealing temperature was reached at heating rates of 10 deg/min. After a 30 min annealing at the respective temperature the sample was cooled with free ends until returning to room temperature at 10 deg/min.

2.2. Characterization methods

2.2.1. Solid state NMR

Solid state NMR measurements were performed in a Bruker MSL300P spectrometer operating at 75.47 MHz for the observation of ^{13}C resonances, using magic-angle spinning (MAS), high-power ^{1}H dipolar decoupling (DD), and ^{1}H–^{13}C cross-polarization (CP) combined techniques. Typical ^{1}H–^{13}C CP contact times were 1–2 ms. In some cases 10 μs or 100 μs were used for better discrimination of the protonated signals. The maximum inter-radio frequency pulse sequence delay was 3.0 s. Spinning rates were selected in the range from 3.3 to 3.4 kHz. The B_1 Radio Frequency field intensity was 55 kHz. The number of scans varied between 200 and 20,000. Glycine signals were employed as external references for determination of the chemical shifts. The temperature of the probe head was set to 20 ± 1 °C.

2.2.2. Synchrotron SAXS and WAXS

Synchrotron radiation ($\lambda = 1.5$ Å) generated at the Soft Condensed Matter Beamline of HASYLAB, Hamburg, Germany was employed working with two basic setups The first setup allowed for consecutive registration of two-dimensional (2D) SAXS patterns and 1D WAXS curves while heating the sample within the 30–240 °C range. The sample-to-detector distance for SAXS was set to 2820 mm, the diffraction patterns being registered by means of a MARCCD 2D detector with exposure times between 30 and 90 s. The 1D WAXS profiles were registered by a linear scintillation detector positioned at a distance of 240 mm in respect to the sample holder. Two-dimensional WAXS patterns were also obtained with selected oriented and isotropic PA6 samples after removing the linear detector and setting the sample-to-MARCCD detector distance to 90 mm.

WAXS and SAXS studies were performed while heating the samples designated as PA6 granules, film and oriented cable. WAXS (1D or 2D) and 2D SAXS images were obtained at temperatures in the 30–240 °C range, reaching the desired temperatures at a heating rate of 20 deg/min. Before taking patterns, the samples were kept at the said temperatures for 30 s. The PA6 granules and the PA6 film were afterwards molten at 240 °C and quenched at a cooling rate of approximately 200 deg/min back to 30 °C where the final X-ray measurement was performed. In the case of PA6 oriented cable, two quenching processes were performed: the first after 200 °C (i.e. before melting), and the second one—after 240 °C, i.e. upon melting and isotropization of the sample.

The X-ray patterns of the PA6 annealed oriented cables were obtained at 30 °C and at the respective temperature.

2.2.3. SAXS and WAXS analyses

To process the 2D WAXS and SAXS images, the X-ray Version 1.0 software was used (Copyright© 1996 by Université Mons Hainaut, Belgium). Corrections for background scattering, irradiated volume and beam intensity were performed for each image. The 2D SAXS patterns were integrated in the range of s values between 0 and 0.15 nm^{-1}, s being the scattering vector, whose modulus is defined as $s = (s_{12}^2 + s_3^2)^{0.5} = (2/\lambda)\sin\theta$.

Bragg long spacings L_B were calculated as the inverse value of s_{max}:

$$L_B = \frac{1}{s_{max}} \tag{1}$$

using the Lorentz corrected SAXS profile after subtraction of the contribution of the liquid scattering. L_B represents the sum of the average thickness of the crystal lamellae, l_c, and of the interlamellar amorphous regions, l_a.

Apparently, equation (1) cannot be used for determination of l_c and l_a. To do that, the approach of Kortleve and Vonk [42] elaborated for the case of isotropic polymers was employed. The Fourier transforms of the Lorentz corrected SAXS profiles were calculated, namely the linear correlation function $\gamma_{1,r,}$ (CF) as:

$$\frac{\gamma_{1,r}}{Q} = \frac{\int_0^\infty (I - I_b) q^2 \cos(qr)\exp(\sigma^2 q^2)\mathrm{d}q}{\int_0^\infty (I - I_b) q^2 \mathrm{d}q} \tag{2}$$

Here, $q = 2\pi s$, I_b is the contribution to the total scattering I arising from density fluctuations in he amorphous phase (liquid scattering), and σ is a term, related to the thickness of the crystal-amorphous interface. Q is the so-called scattering invariant that can be determined by integrating the

SAXS profile over all scattering angles, i.e.:

$$Q = \int_0^\infty (I - I_b) q^2 \mathrm{d}q \tag{3}$$

The advantage of the CF over the Bragg's law is that, in addition to the long period L, values for l_a, l_c and the degree of crystallinity within the lamellar stacks x_{cl}, (the so-called 'linear crystallinity') can be obtained [42–44].

For elimination of I_b contribution in the raw SAXS profile, for the Lorentz correction of the latter and for calculation of the linear CF, the SASDAP software (Copyright© 1995 by Verma, Biswas and Hsiao, DuPont Experimental Station, Wilmington, DE, USA) was used. Apart from the L_B value, SASDAP calculates for each sample two additional estimates for the long spacing—from the position of the first maximum of CF (denoted as L_c^M) and from twice the position of the first minimum of CF (L_c^m). To calculate the values of l_c and l_a on the basis of CF, we used the procedure described in ref. [45] based on the following equation:

$$\frac{B}{L_c^M} = x_1(1 - x_1) \tag{4}$$

where B is the position of the first intercept of CF with the r-axis. From the two solutions $x_{1,2}$ of the above quadratic equation, the one with the higher value is ascribed to the larger fraction of the two phases found within the lamellar stacks. For example, in highly crystalline samples, x_1 would correspond to the crystal fraction within the lamellar stacks (i.e. x_{cl},) and $1-x_{cl}$ would, then, represent the amorphous fraction within the stack.

Once the assignment of x_{cl} is made, one may calculate the l_a and l_c from the values of L employing the following equations:

$$l_c = x_{cl} L \text{ and } l_a = (1 - x_{cl}) L \tag{5}$$

where L, as indicated in [44,45], may take the values of L_c^M, or L_c^m.

The 1D WAXS curves were processed by OTOKO software (Copyright© by Koch, HASYLAB, Hamburg). Their scattering angle axis was calibrated using the angular position of the reflections of a standard crystalline poly(ethylene terephthalate) sample. The WAXS curves obtained from all four sets of PA6 samples were deconvoluted according to the procedure described in Ref. [27] by fitting to them of five Gaussian peaks–four crystalline and one amorphous. In increasing order of their 2θ position, the four crystalline peaks can be ascribed to α[200], γ[001], γ[200] and α[002/202] crystal plane diffractions [27]. In isotropic PA6 samples (PA6 granules and PA6 film), deconvolution of the 1D WAXS curves allowed the calculation of the total degree of crystallinity (or, crystallinity index, CI) as a relation of the areas of all crystalline peaks and the total area underneath the WAXS curve:

$$\mathrm{CI} = \frac{\sum A_c}{\sum (A_c + A_a)} \tag{6}$$

where A_c is the integrated area underneath the respective crystalline peaks and A_a is the integrated area of the amorphous halo.

In oriented PA6 samples, the intensity of the meridional point-like reflections cannot be determined from the 1D WAXS curves, which is an equatorial cut of the WAXS pattern. Therefore, in this case, ΣA_c in Eq. (1) will measure the scattering intensity along the equator only, i.e. one can define it as 'equatorial crystallinity index' (ECI). Obviously, ECI cannot be considered a measure for the absolute crystallinity of the oriented samples, but can be used to compare them for qualitative trends.

The WAXS patterns were used also to determine the unit cell parameters calculating the d-spacings (d_{hkl}) using the Bragg's law:

$$2d_{hkl} \sin\theta = n\lambda \tag{7}$$

There, λ is the X-ray wavelength, θ is the half of the 2θ position of the center of the respective crystalline peak, n is an integer ($n=1,2,3,\ldots$) depending on the order of the given plane related to the respective peak. Hence, if in Eq. (2) the peak of the [200] crystalline plane is used to calculate the d_{200} of a certain crystalline form, n becomes 2 and the Bragg's law gives the a-edge of the unit cell. The c-edge of the α and γ-unit cells of PA6 was calculated from the α002/202 and γ001 crystalline planes, respectively. In the case of oriented samples, the two reflections on the meridian of the 2D WAXS patterns are ascribed to the scattering of the γ[020] crystalline plane [27]. Performing meridional cuts of the corresponding images, the angular position of the γ[020] crystalline plane was established and used for the calculation of the b edge of the γ-unit cell.

3. Results

3.1. Solid-state NMR measurements

CP-DD/MAS ^{13}C-NMR spectra of PA6 granules, film, oriented cable and oriented cable annealed at 200 °C were obtained and analyzed. The full-range spectra of all PA6 samples are of the type represented in Fig. 1(a). The multiple peaks observed in the 20–50 ppm range belong to the aliphatic carbon atoms. The resonance lines centered close to 173 ppm originate from the carbonyl C-atoms. Each full-range spectrum contains also two spinning side bands, which are due to the larger chemical shift anisotropy of the carbonyl groups. Fig. 1(b)–(e) show the extended aliphatic carbon regions of the four samples. The data for the chemical shifts are summarized in Table 1. The same table contains also the chemical shifts of the carbon atoms of α and γ-crystalline forms of PA6 as given in Ref. [46].

Comparing the solid state NMR data of α and

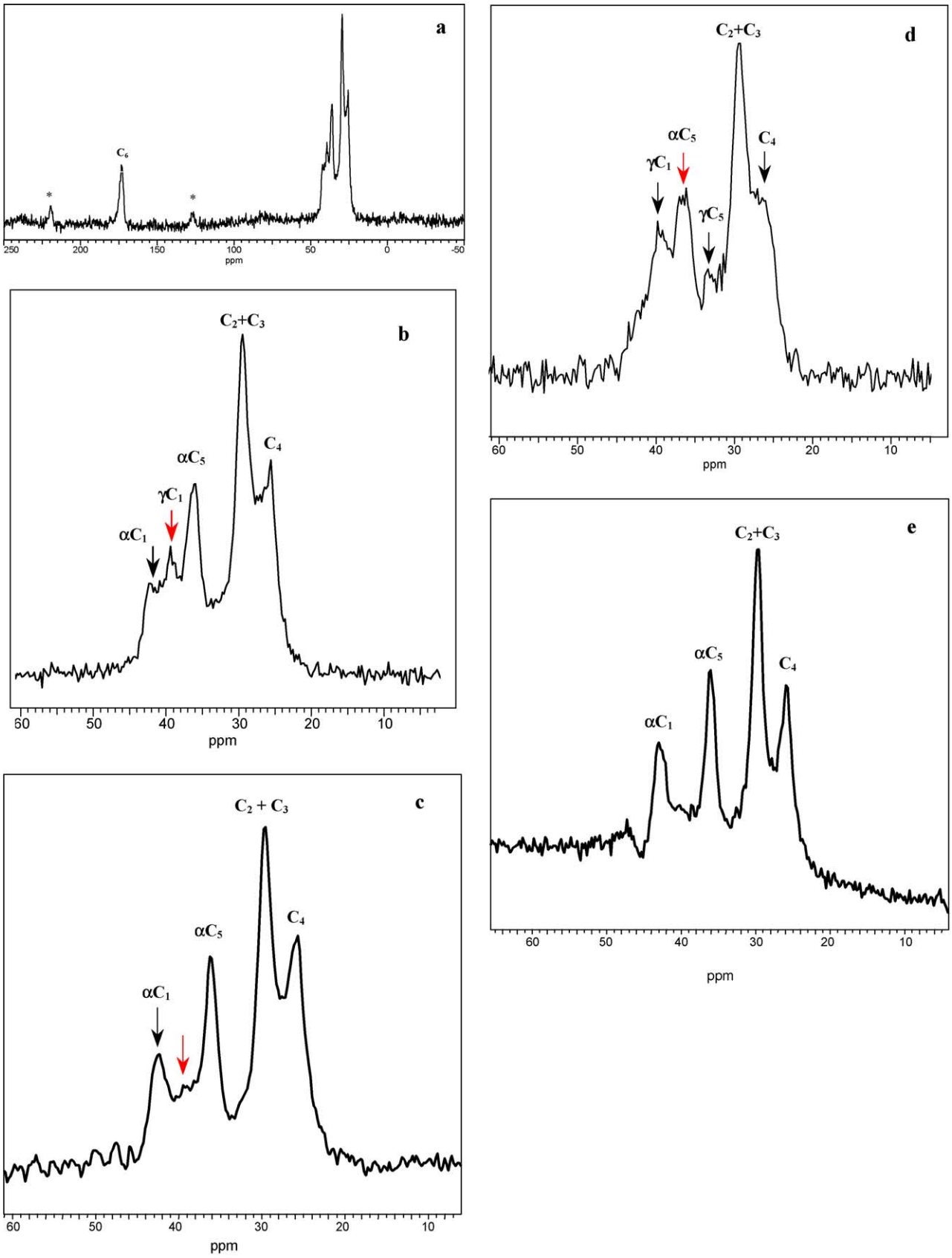

Fig. 1. ^{13}C CP-MAS NMR spectra of PA6 samples at 20 °C. (a) PA6 granules, full range. Asterisks denote spinning sidebands; (b) PA6 granules, magnification of the aliphatic carbons region; (c) PA6 film; (d) PA6 oriented cable; (e) PA6 oriented cable after 30 min annealing at 200 °C.

Table 1
Chemical shifts (ppm) registered for the carbons in the ^{13}C solid state NMR spectra of PA6 granules, PA6 film, PA6 oriented cable and PA6 oriented cable annealed for 30 min at 200 °C

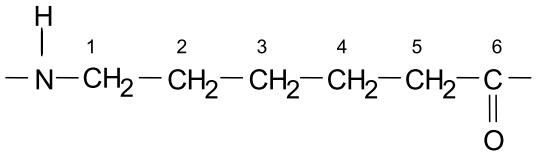

Sample	Chemical shifts of carbons (ppm)				
	C_1	C_2+C_3	C_4	C_5	C_6
α-PA6[a]	42.6	30.0	26.0	36.4	173.4
γ-PA6[a]	39.9	29.8	26.4	33.6	173.4
PA6 granules	42.2; 39.4	29.5	25.6	35.9	173.4
PA6 film	42.3	29.4	25.7	36.3	173.0
PA6 oriented cable	39.8	29.2	26.0	33.3; 36.5	172.5
PA6 oriented annealed at 200 °C	42.9	29.6	25.9	36.1	172.8

All the spectra are taken at room temperature. Literature data of α and γ-PA6 are given for comparison.
[a] According to Ref. [46].

γ-crystalline forms of PA6 (Table 1), one may conclude that the chemical shifts of $\alpha(C_2+C_3)$, αC_4, αC_6 almost coincide with those of the corresponding γ-PA6 carbons. At the same time, the C_1 and C_5 chemical shifts of the α-form show a difference of almost 3 ppm as compared to those of the γ-form. Most probably, this effect is due to the different geometry and orientation of the H-bonds realized between the amide groups in α and γ-PA6. Hence, the C_1 and C_5 resonance lines of PA6 samples can be used to make a distinction between the two crystalline forms.

Having in mind the chemical shifts data of pure α and γ-forms of PA6, the peaks at 42.2, 29.5, 25.6, 35.9 and 173.4 ppm (Table 1) observed in the spectrum of the PA6 granules should be assigned to the αC_1, (C_2+C_3), C_4, αC_5 and C_6 chemical shifts, respectively. The resonance registered at 39.4 ppm found in the same sample (Fig. 1(b)) belongs to a γC_1 carbon. No peak for the γC_5 resonance was observed in this spectrum.

In the PA6 film (Table 1), all the resonances observed correspond to the carbon atoms of the α-form PA6. As seen from Fig. 1(c), there is also a low-intensity shoulder centered between 39 and 40 ppm that can be attributed to the γC_1 carbon.

In the PA6 oriented cable (Table 1, Fig. 1(d)) the bands at 39.8, 29.2, 26.0, 33.3 and 172.5 ppm are attributable to the γC_1, (C_2+C_3), C_4, γC_5 and C_6 chemical shifts, respectively. In this sample, there is an additional peak at 36.5 ppm that corresponds to the C_5 chemical shift of α-PA6 but at the same time the αC_1 resonance line is missing.

The spectrum of the PA6 oriented cable previously annealed for 30 min at 200 °C (Fig. 1(e), Table 1) shows clear carbon resonance lines of PA6 in α-form. Similarly to spectrum of the PA6 film, in the 39–40 ppm range there is a very weak γC_1 signal.

Summarizing the solid state NMR data, it can be concluded that the four PA6 samples do not represent pure α or γ-PA6 crystalline modifications but are mixtures of the two forms whose content depends on the previous treatment.

3.2. SAXS measurements

Selected 2D SAXS patterns are shown in Fig. 2(a)–(e). The images obtained with the PA6 granules or with the isotropic PA6 film were similar to the patterns in Fig. 2(a) and (e). The oriented PA6 samples showed different SAXS patterns depending on their thermal history. The as-drawn cable heated in the 30–160 °C range while irradiated showed patterns similar to Fig. 2(b) presenting spots whose intensity increased with temperature. Close to the Brill transition (195–200 °C), two-point diagrams similar to Fig. 2(c) were registered. Prolonged annealing at 200 °C followed by slow cooling to 30 °C gives rise to a different crystalline structure and perfection, as seen from Fig. 2(d). Heating up to 240 °C led to a complete loss of orientation in the PA6 cables, which was visualized by SAXS patterns of circular symmetry (Fig. 2(e)).

Fig. 3 displays the set of CFs calculated for PA6 granules heated in-beam at 120, 160 and 200 °C (curves 1–3, respectively), as well as at 30 °C after melting the granules (curve 4). The structural data extracted by correlation function analysis from all the four PA6 samples as a function of temperature are presented in Table 2. It should be noted that in the raw SAXS profiles of PA6 granules at 30 and 90 °C, the s_{max} values were so high that calculation of the corrected L_B values was only possible. No estimates for B, L_c^m and L_c^M and $x_{cl.}$are presented for the oriented PA6 samples, either. To obtain correct and comparable data in this case, more sophisticated calculation procedures are needed, such as the Chord Distribution Function (CDF) [47].

It can be seen from Table 2 that increasing the temperature results in a general increase of the initial L_B values. The latter are dependent on the sample orientation

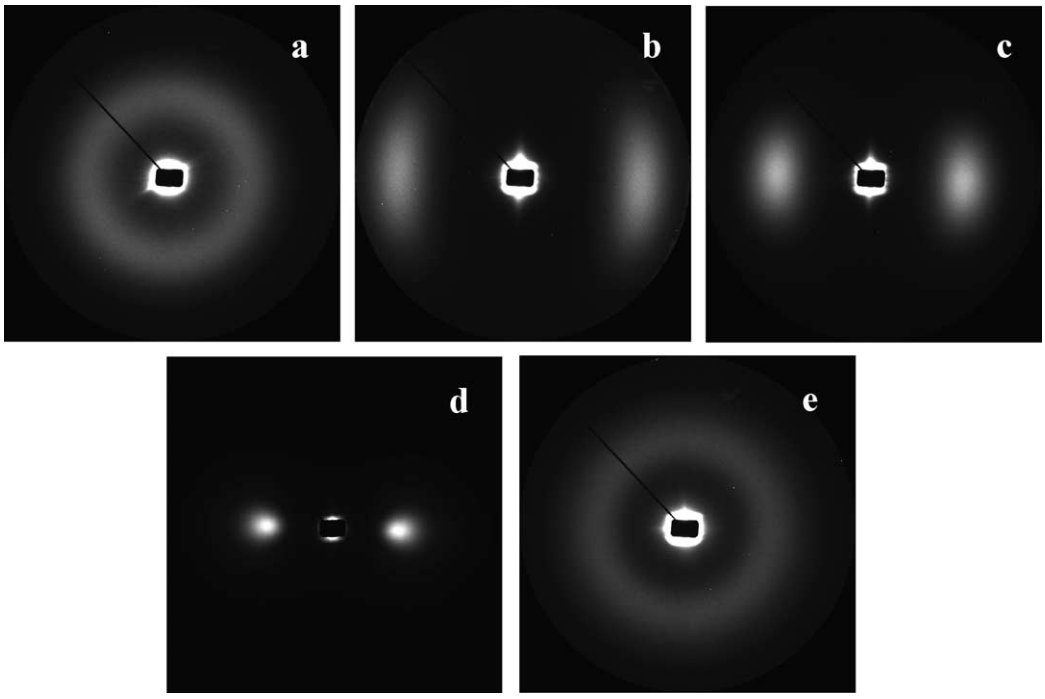

Fig. 2. Selected 2D SAXS patterns of PA6: (a) PA6 granules at 160 °C; (b) oriented PA6 cable heated in-beam at 160 °C; (c) oriented PA6 cable heated in beam at 200 °C; (d) oriented cable annealed for 30 min at 200 °C, image taken at 30 °C; (e) sample (c) after isotropization at 240 °C, image taken at 30 °C. Note: the draw direction in oriented samples is horizontal.

and pre-treatment and are the largest in the case of PA6 film. Fast cooling results in some depression of the long spacing estimates, as well as of the x_{cl} values.

3.3. WAXS measurements

Selected representative examples of 2D WAXS patterns of isotropic and oriented PA6 samples are displayed in Fig. 4. The draw direction DD (i.e. the fiber axis) in all oriented images is vertical. The PA6 granules (Fig. 4(a)–(c) show 2D patterns of circular symmetry with a clear change from one (samples at 30 and 200 °C) to two Debye rings (30 °C after heating to 240 °C and fast cooling), indicative of changes in the crystalline structure. The patterns of the oriented PA6 samples (Fig. 4(d)–(f)) contain equatorial reflections (arcs) being perpendicular to DD, as well as meridional point-like reflections parallel to DD. There is a visible variation in the intensity distribution, form and number of equatorial reflections as the temperature of the measurement changes, which variation has to be related with structural alterations in the crystalline phase. The difference in intensity of the two meridional reflections in the oriented patterns should be attributed to a slight tilt of the sample holder.

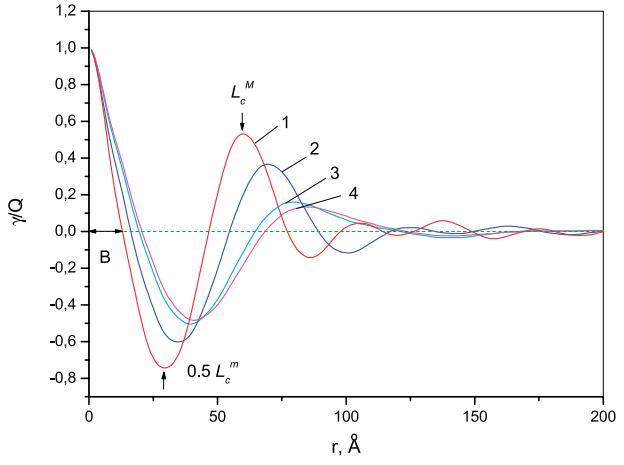

Fig. 3. Linear correlation function curves calculated from the SAXS patterns of PA6 granules obtained at: 1–120 °C; 2–160 °C; 3–200 °C; 4–30 °C after melting at 240 °C. The arrows indicate the positions of B, L_c^m and L_c^M parameters for curve 1.

To quantify the content of α and γ-crystalline forms, 1D WAXS patterns were obtained and deconvoluted. Some of the fitted 1D WAXS curves are represented in Fig. 5. As suggested by many authors, a monoclinic unit cell lattice was assumed for the α-PA6 form characterized by two peaks corresponding to α[200] and α[002/202] crystalline planes with 2θ being between 19 and 20° and 23 and 24°, respectively. For the γ-crystalline form, non-hexagonal unit cell was initially supposed for all samples, as suggested in Ref. [27], i.e. fits with two Gaussian peaks corresponding to γ[001] and γ[200] crystalline planes were performed with 2θ being between 21 and 22°. These two suppositions for the α and γ-type crystalline lattice led to excellent fits with fitting coefficients $r^2 \geqq 0.999$. However, in the case of PA6 film irradiated at 30 °C (Fig. 5(b)) as well as for all samples quenched after melting, the fit was made with two Gaussians

Table 2
Structural parameters extracted by analysis of the SAXS profiles of PA6 samples with various mechanical and thermal pre-history

Temperature of the measurement (°C)	L_B,[a] (Å)	L_c^M, (Å)	L_c^m, (Å)	l_c, (Å)	l_a, (Å)	x_{cl}
PA6 granules (in-beam heating)						
30	52	–[b]	–	–	–	–
90	58	–[b]	–	–	–	–
120	61	60	60	41	19	0.677
160	72	70	70	44	26	0.622
200	94	86	82	51	35	0.589
30 after 240	89	79	78	43	36	0.542
PA6 film (in-beam heating)						
30	82	80	80	51	29	0.634
90	82	80	80	51	29	0.640
120	82	80	80	50	30	0.621
160	85	82	80	50	32	0.636
200	99	92	90	63	29	0.680
215	137	134	114	91	43	0.680
30 after 240	90	84	84	50	34	0.600
PA6 oriented cable (in-beam heating)[c]						
30	57	–	–	–	–	–
120	61	–	–	–	–	–
160	64	–	–	–	–	–
200	85	–	–	–	–	–
30 after 240	87	78	78	47	31	0.608
PA6 oriented cable (hot-stage annealing)[c]						
120	59	–	–	–	–	–
160	62	–	–	–	–	–
200	109	–	–	–	–	–

[a] Calculated after Lorentz correction of the raw SAXS pattern and subtraction of I_b
[b] Calculation of the linear CF impossible due to large s_{max} values.
[c] Correct values for l_c, l_a and x_{cl} in oriented samples cannot be calculated from the linear CF, see the text.

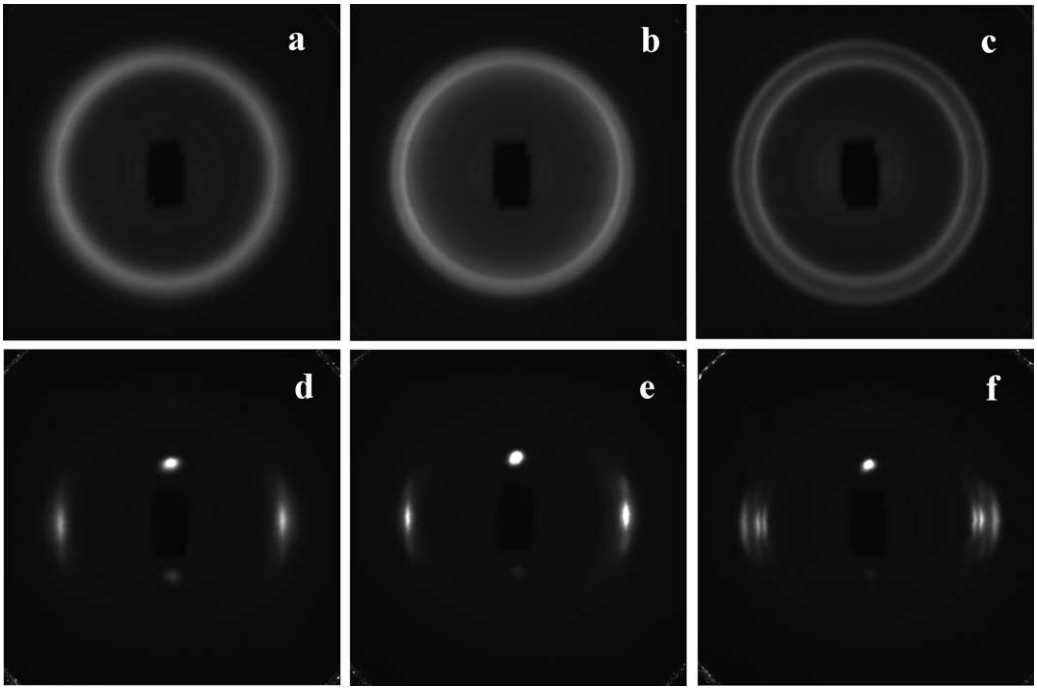

Fig. 4. Selected 2D WAXS patterns of PA6 samples: (a) PA6 starting granules at 30 °C; (b) granules at 200 °C; (c) granules at 30 °C after melting at 240 °C; (d) as-drawn oriented cable at 30 °C; (e) oriented cable at 200 °C; (f) oriented cable at 30 °C after 200 °C. Note: the draw direction in the oriented samples is vertical.

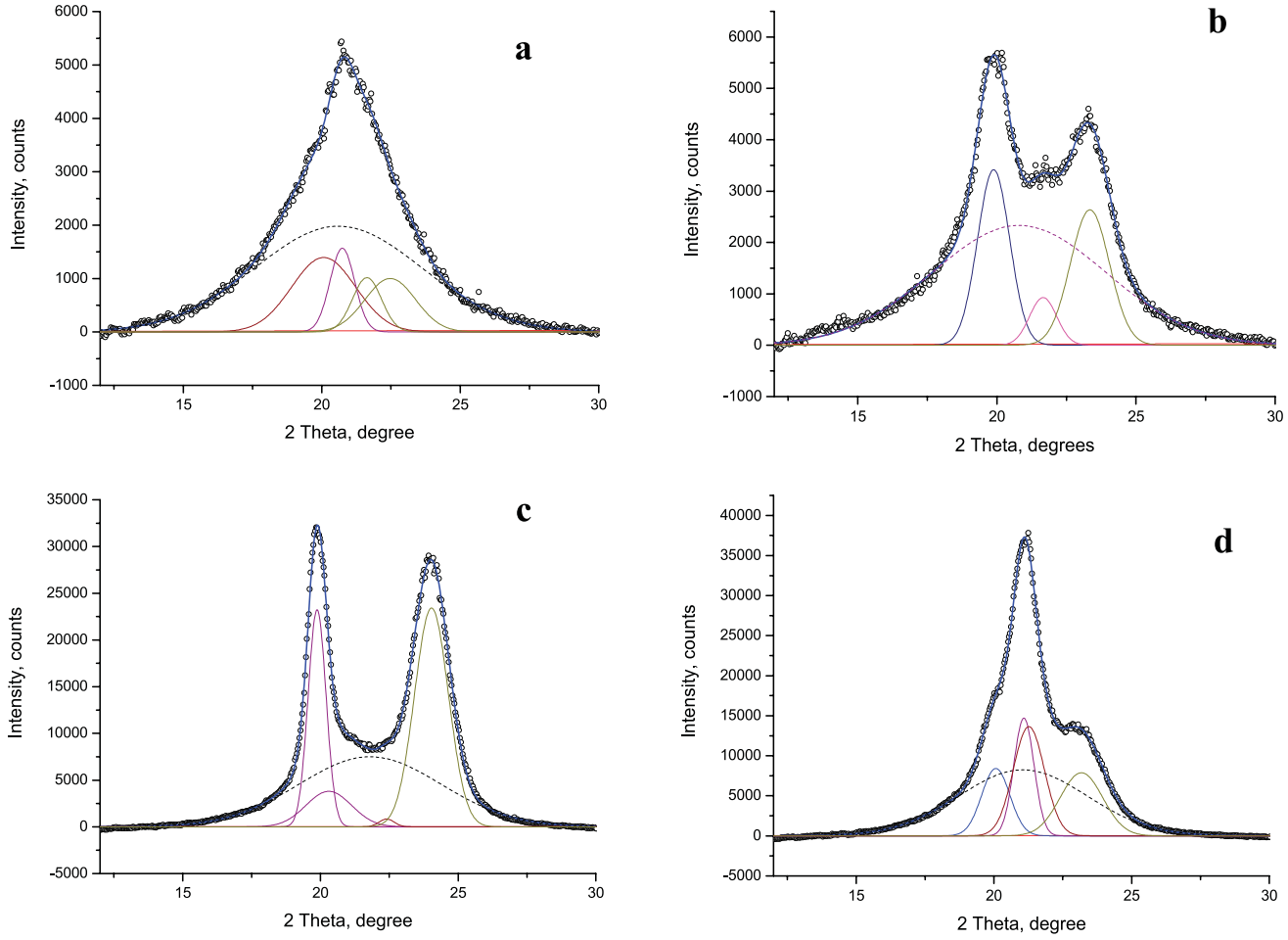

Fig. 5. Selected 1D WAXS patterns of isotropic and oriented PA6 samples and their deconvolution: (a) PA6 starting granules at 30 °C; (b) PA6 film at 30 °C; (c) PA6 oriented cable annealed at 200 °C, pattern obtained at 30 °C; (d) PA6 oriented cable after heating at 200 °C and quenching to 30 °C, pattern obtained at 30 °C. Note: crystalline peaks are given by solid lines, the amorphous halo—by dashed lines.

for the α-form and one for the γ-form. Any attempt to introduce a second Gaussian for the γ-form led to fitting coefficients inferior to 0.98. This is a sign that a hexagonal γ-lattice is most probably formed in the last cases.

Tables 3–5 contain the changes in α and γ-form content, CI and ECI of the three PA6 samples as a function of temperature. Their unit cell edges *a*, *b* (in oriented PA6 samples only) and *c* were also calculated and presented in Table 6. These data will be discussed in the next section.

4. Discussion

The four PA6 samples with different thermal and mechanical pre-histories were prepared and characterized under various temperature conditions so as to model the structural changes of the polyamide reinforcing phase during the consecutive stages of MFC preparation. They include melt-mixing at 240–250 °C, quenching and cold-drawing of the blend, selective melting of the matrix phase

Table 3
Temperature dependence of the total crystallinity index CI, α and γCIs in PA6 granules heated in the X-ray beam at a heating rate of 20 deg/min

Heat treatment (°C)	α_{200} (%)	$\alpha_{002}/\alpha_{202}$ (%)	αCI (%)	γ_{001} (%)	γ_{200} (%)	γCI (%)	CI (%)
30	16.5	9.5	26.0	7.2	5.5	12.7	38.7
120	20.4	3.5	23.7	7.1	7.4	14.5	38.2
160	10.7	8.6	19.3	7.2	12.0	19.2	38.5
200	4.2	19.8	24.0	5.5	6.2	11.7	35.7
30 after 240	17.1	16.2	33.3	–	3.1	3.1	36.4

(CI = αCI + γCI). Note: images taken 30 s after reaching the respective temperature.

Table 4
Temperature dependence of the total crystallinity index CI, α and γCIs in PA6 film heated in the X-ray beam at heating rate of 20 deg/min

Heat treatment (°C)	$\alpha_{200\%}$	$\alpha_{002}/\alpha_{202\%}$	αCI %	γ_{001} (%)	γ_{200} (%)	γCI (%)	CI_{Total} (%)
30	17.1	16.0	33.1	–	3.9	3.9	37.0
90	11.6	19.9	31.5	10.1	1.7	11.8	43.3
120	12.9	11.8	24.7	12.3	8.8	21.1	45.8
160	17.9	7.2	25.1	7.8	9.7	17.5	42.6
195	12.6	5.6	18.2	7.8	10.1	17.9	36.1
200	10.0	9.1	19.1	5.9	12.1	18.0	37.1
215	9.7	15.3	25.0	2.0	6.5	8.5	33.5
30 after 240	19.5	17.3	36.8	–	3.8	3.8	40.6

(CI = αCI + γCI). Note: images taken 30 s after reaching the respective temperature.

in the 150–200 °C range, and cooling back to room temperature. For the sake of clarity, the data sets for each particular PA6 sample will be discussed separately.

4.1. PA6 granules

As seen from the solid state NMR traces (Table 1), there is a co-existence of α and γ-PA6 forms. However, the CP-DD/MAS technique employed does not permit ultimate conclusions about the exact ratio between the two crystalline forms. Nevertheless, based on the fact that the shape of the NMR spectrum (Fig. 1(a) and (b)) is more like the one of the pure α-PA6 form [46] and considering the presence of clear resonance line only for the γC_1 and not for the γC_5, it may be supposed that this sample is predominantly in α-crystalline form with lower content of γ-PA6.

A confirmation of the above supposition comes from Table 3, which shows data about the concentration of α-, γ-crystalline forms and the total CI as a function of temperature. In PA6 granules at 30 °C with a CI of 39%, there is more α than γ-type crystallinity, their relation being close to 2:1. This is in agreement with the NMR data evidencing that PA6 granules are predominantly in α-form. It may also be seen from data in Table 3 that a transition from α to γ-form occurs between 120 and 160 °C, the two crystalline forms showing almost identical concentrations at 160 °C. Between 160 and 200 °C, however, the trend reverses, i.e. the transition becomes from γ to α-PA6 form.

The long spacing estimates L_B, L_c^M, and L_c^m grow as the temperature increases in the 30–200 °C range, whereas the linear crystallinity x_{cl} decreases (Table 2). This results in a stronger enlargement of l_a as compared to that of l_c. Since the CI remains almost constant, it may be concluded that no additional crystallization or melting process takes place throughout the entire temperature interval. The said changes in l_c, l_a and long spacing estimates can therefore be related to the phase-to-phase transitions, as well as to possible thermal expansion. The data from Table 6 show that the unit cell edges of both α and γ-form PA6 granules generally grow with the temperature. The increase of the d-spacings is different. The strongest growth is registered with the d-spacings of α[200] and γ[001], with 7 and 4%, respectively. These two d-spacings roughly correspond to the inter-planar spacing along the H-bonds direction in α and γ-PA6, respectively. On the other hand, the smallest increased is shown by the d-spacings of α([002]/[202]) and γ[200] planes, which characterize the direction of the van der Waals forces in the two forms. The observed increase in the unit cell edges is in accordance to the supposed thermal expansion. Clearly then, decreasing the temperature will be expected to diminish the unite cell edges and the l_c estimates, which was really observed when the sample was quenched to 30 °C after melting (Table 6, Table 2). As seen from Eq. (5), additional decrease in l_c will also results from the decline in the linear crystallinity x_{cl} within the stack, which is a fact during quenching (Table 2). At the same time, l_a remains similar to that at 200 °C. In other words, quenching results in 'freezing' of the amorphous phase thickness, whereas the crystalline phase undergoes several changes. First of all, there occurs a volume contraction due to the reduced temperature. Second, formation of crystallites predominantly in α-form takes place, with the

Table 5
Temperature dependence of the equatorial crystallinity index ECI, α and γECIs in PA6 oriented cable heated in the X-ray beam at heating rate of 20 deg/min

Heat treatment (°C)	α_{200} (%)	$\alpha_{002}/\alpha_{202}$ (%)	αECI (%)	γ_{001} (%)	γ_{200} (%)	γECI (%)	ECI (%)
30	8.1	9.8	17.9	12.3	18.1	30.4	48.3
120	8.6	10.2	18.8	16.4	12.0	28.4	47.2
160	12.9	11.6	24.5	9.7	13.7	23.4	47.9
200	18.3	19.1	37.4	8.4	8.8	17.2	54.6
30 after 200	11.1	14.0	25.1	28.1	2.6	30.7	55.8
30 after 240	21.5	15.8	37.3	–	0.7	0.7	38.0

(ECI = αECI + γECI). Note: images taken 30 s after reaching the respective temperature.

Table 6
Unit cell parameters of the α and γ-crystalline forms in PA6 granules, PA6 film and PA6 oriented cable as a function of temperature. The b-edge direction coincides with the chain axis

Temperature (°C)	PA6 granules				PA6 film				PA6 oriented cable				
	d_{200} a_α, Å	d_{002}/d_{202} c_α, Å	d_{200} a_γ, Å	d_{001} c_γ, Å	d_{200} a_α, Å	d_{002}/d_{202} c_α, Å	d_{200} a_γ, Å	d_{001} c_γ, Å	d_{200} a_α, Å	d_{002}/d_{202} c_α, Å	d_{200} a_γ, Å	d_{001} c_γ, Å	d_{020} b_γ, Å
30	8.61	7.70	7.99	4.17	8.69	7.42	7.98*	3.99*	8.68	7.76	8.15	4.15	14.92
120	8.53	7.63	8.03	4.18	8.87	7.70	7.90	4.20	8.68	7.86	8.19	4.18	14.8
160	8.84	7.78	8.14	4.20	8.67	7.82	8.06	4.19	8.64	8.04	8.27	4.20	14.92
195	–	–	–	–	8.89	7.87	8.16	4.19	–	–	–	–	–
200	9.22	7.96	8.39	4.32	9.01	7.92	8.28	4.19	8.60	8.15	8.27	4.21	14.92
215	–	–	–	–	9.17	7.95	8.42	4.35	–	–	–	–	–
30 after 200	–	–	–	–	–	–	–	–	8.61	7.47	7.85	3.93	15.44
30 after 240	8.54	7.47	7.99[a]	4.0[a]	8.65	7.41	7.94[a]	3.97[a]	8.52	7.57	7.96[a]	3.98*	–

[a] Hexagonal γ-form

ratio between the α and γ-PA6 forms reaching 10:1 (Table 3). This is contrary to some previous reports [31,35–37] stating that rapid cooling favors the formation of γ-crystallites. Third, the remaining γ-form suffers modification. During the heating in the entire 30–200 °C range this crystalline form is non-hexagonal, as it can be seen from Table 3, supposedly with monoclinic lattice as previously described by some authors [41], or with orthorhombic one, which is the minimum requirement to generate two reflections. Quenching after melting, however, changes the γ-PA6 lattice into hexagonal, i.e. it shows only one reflection with 2θ at about 20–21°. Similar changes in the lattice type of PA6 γ-phase upon cooling were reported previously [48].

4.2. PA6 film

Based on the NMR data (Table 1, Fig. 1(c)), it can be considered that the PA6 film contains predominantly the α-crystalline modification with some minor admixtures of γ-form. Analyzing 1D WAXS traces by deconvolution confirms that, in fact, the α-form content in the initial film at 30 °C is about ten times larger than that of the γ-form (Table 4), whereby the latter is characterized by a hexagonal lattice of its unit cell (Fig. 5(b)).

Increasing the temperature provokes phase-to-phase transitions, as seen from the data in Table 5. Similarly to the PA6 granules, initially a transition from α to γ-crystalline form takes place, which trend reverses at about 200 °C. Another observation is that the CI in PA6 film varies in the whole temperature interval. It grows until 120 °C and decreases between 120 and 215 °C, thus indicating that an additional crystallization or melting most probably occur along with the phase-to-phase transition.

Table 2 shows the long spacings estimates L_B, L_c^M, and L_c^m as a function of the temperature. The PA6 film at 30 °C displays a long spacing that is notably larger than that in the PA6 granules. This fact may be explained with the way the PA6 film was prepared including compression molding of granules at 250 °C followed by a relatively rapid cooling to room temperature, which can be considered as non-isothermal annealing. As previously observed, annealing of PA6 always results in a growth of its long spacing values [49]. Increasing the temperature up to 160 °C does not cause changes in L_B, L_c^M, and L_c^m. Since at the same time CI increases, one may suppose that this effect is related with the formation of new crystallites and not with thickening of the existing lamellae. Above 160 °C, however, long spacings, as well as l_c and l_a start to grow, this trend being better expressed in the 200–215 °C range. Having in mind that the content of the α-form increases whereas that of the γ-form decreases which is accompanied by a CI reduction (Table 4), it may be concluded that in this temperature range the γ to α-phase transition mentioned above is accompanied by melting of some crystallites mainly of γ-type.

All unit cell edges of α and γ-crystalline lattice of PA6 film grow when the temperature increases from 30 to 215 °C (Table 6). Here, the strongest expansion is along the van der Waals forces direction in α-form and the H-bond direction in γ-form, corresponding to the d-spacings of α[002]/[[202] and γ[001], respectively As it may be seen from Table 6, these changes in the unit cell are reversible. Quenching to 30 °C after melting restores the initial dimensions of the unit cell. Just like in the case of the granules, this rapid cooling leads to the formation of PA6 mainly in α-crystalline modification (Table 4). The small amounts of the remaining γ-crystallites are with hexagonal unit cell, i.e. a structure similar to the initial PA6 film is realized. Again, the x_{cl} value after quenching is the lowest (Table 2).

4.3. PA6 oriented cable

PA6 oriented cable also represents a mixture of α and γ-crystalline modifications. Contrary to the previously studied two isotropic samples, the cable shows the presence predominantly of γ-form. The CP-DD/MAS ^{13}C NMR analysis of this sample (Fig. 1(d), Table 1) shows clear peaks for γC_1 and γC_5 with lower content of the α-form (αC_5 resonance only). Having in mind that the oriented sample was prepared from isotropic granules mostly in α-form, one can conclude that melting of PA6 followed by cold drawing favored the formation of γ-form. The NMR spectra of PA6 cable shows also that the resonance line of the carbonyl C-atom (C_6) appears in slightly stronger fields (below 173.0 ppm) than the one of the non-oriented samples (Table 1). Most probably, upon cold drawing of PA6, a conformation with more electron-shielded carbonyl atom is realized, which can be the consequence of a closer packing of the PA6 macromolecules.

Deconvolution of the respective 1D WAXS curves confirms that in the initial oriented PA6 cable at 30 °C there is more γ than α-crystalline phase, their relation being 1.7:1.0, respectively (Table 5). The starting ECI at 30 °C in this sample is 48%, i.e. with about 10% higher than the CIs of the two isotropic PA6 samples at the same temperature. Actually, the difference is even larger, because the intensity of the meridional γ[020] reflection is not taken into consideration in the ECI calculation. Most probably, the higher crystallinity in the PA6 cable should be attributed to its strong orientation (DR = 15) obtained by cold drawing.

Increasing the temperature above 120 °C results in a transition from γ to α-PA6 crystalline modification. At 160 °C the two forms reach almost equal concentrations (about 24%). In view of the fact that in the 120–160 °C range both ECI and L_B values remain almost constant (Table 5, Table 2), one can suppose that there is no additional melting or crystallization in this temperature range. Above 160 °C, the γ to α-transition continues and at 200 °C the relation becomes 2:1, now in favor of the α-form. At the same time, ECI increases from 48 to 55%. This means that additional crystallization of amorphous material into α-crystallites takes place in the temperature range between 160 and 200 °C, which was not the case with the two isotropic PA6 samples. This augmentation of ECI is accompanied by a growth of L_B by approximately 20 Å in the 160–200 °C range. It was not possible to determine the discrete contribution of l_c and l_a to the said growth of the L_B at high temperatures. As mentioned above, in samples with fiber symmetry (i.e. a two-dimensional system), correct structural parameters cannot be extracted by calculating and analyzing the linear CF or the Ruland's interface distribution functions, which are valid in non-oriented (one-dimensional) systems. That is the reason that Table 2 contains only Bragg's long spacings for the PA6 oriented cable. Nevertheless, having in mind that the ECI grows, it can be supposed that the L_B increase should be attributed to thickening of the crystalline lamellae, i.e. to a growth of l_c mainly. Contrary to the thermal expansion, the said thickening should not be reversible when cooling down. As seen from Table 2, PA6 cable after quenching displays even larger L_B value, as compared to that at 200 °C, which corroborates the above supposition.

Table 6 contains data about α-and γ-form unit-cell edges in PA6 cable as a function of temperature. The *b*-edges of the γ-form lattice in this sample were obtained from the diffraction peak of γ[020] plane in the 2D WAXS patterns as described in Section 2. One can see that the *b*-edge of the γ-form remains unchanged until 200 °C indicating that there is not lattice expansion in the direction of the polymer chains. The biggest growth here (ca. 5%) is of the interplanar distance along the direction of the van der Waals forces in α-form. At the same time, there is no increase of the *a*-edge of the α-form, which even slightly decreases at 200 °C. The rest of the d-spacings grow by less than 1%, which is one more fact indicating that in PA6 oriented cable the increase in L_B cannot be explained mainly with thermal expansion, as in the cases of the two isotropic samples.

It was interesting to follow the structural changes in the PA6 cable upon quenching to 30 °C before and after melting. As expected, quenching before reaching the melting point does not upset the orientation of the sample (Fig. 4(f)). It leads to the formation of a mixture of α and γ-forms with a slight excess of the latter (1.00:1.22), whereby the γ form lattice continues non-hexagonal as in the starting PA6 cable at 30 °C. However, if the quenching is performed after melting at 240 °C, the sample looses its orientation and the PA6 crystalline phase transforms almost quantitatively into α-modification. There are only traces of γ-form (less than 1%), which is with hexagonal lattice (Tables 5). As seen from Table 6, quenching of PA6 cable leads to smaller *a* and *c* edges for the two crystalline forms, which means smaller distances between the macromolecules in the plane of the sheet, as well as shorter inter-sheet distances. This would mean that quenching is related to the formation of smaller crystallites of both α and γ-type with closer packing between the macromolecules.

Interestingly enough, quenching of the PA6 cable before

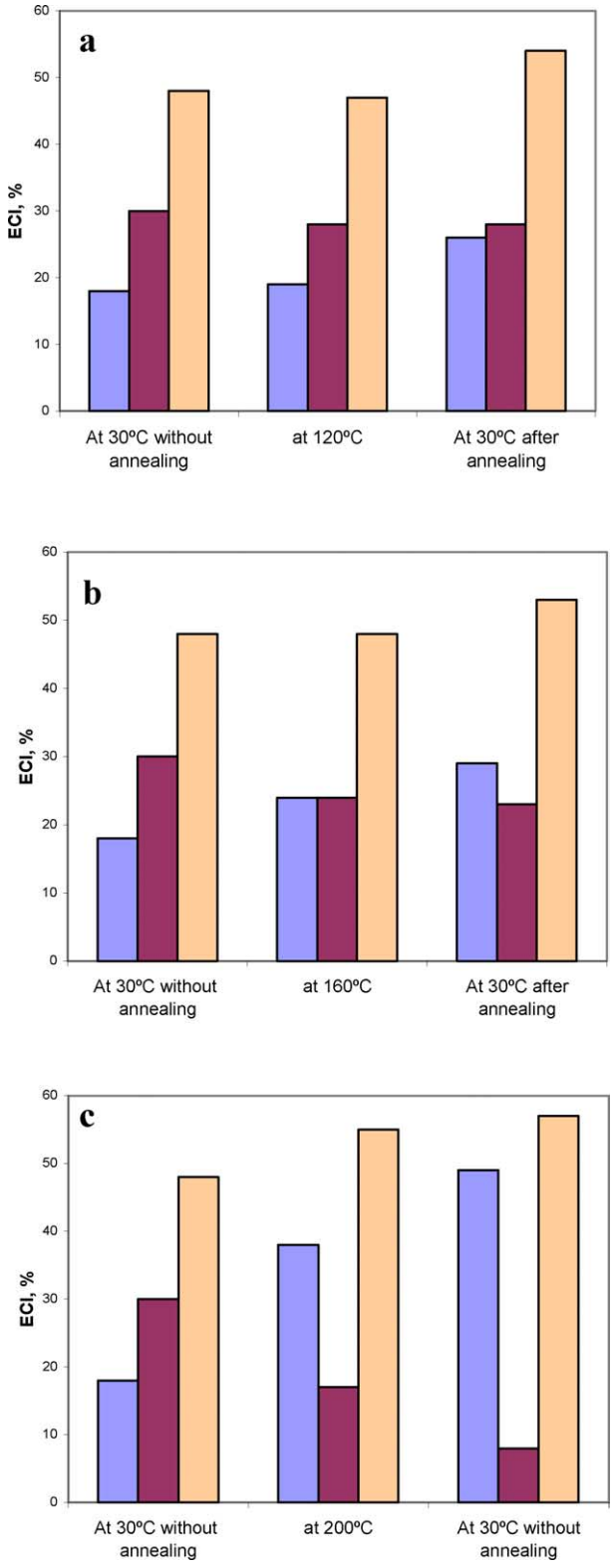

Fig. 6. ECI and its α and γ-components in PA6 oriented cable as a function of annealing temperature: (a) 120 °C; (b) 160 °C; (c) 200 °C. ■ α-form concentration; ■ γ-form concentration; ■ ECI.

melting leads to a *b*-edge of the γ-form being with 3.5% higher than the starting value (Table 6). In this case the γ-modification seems to contain more stretched macromolecules.

4.4. Annealed PA6 cable

Fig. 6(a)–(c) displays the changes in ECI and the comparison between the amounts of the two crystalline forms in PA6 cables before any heat treatment, at a certain temperature (120, 160 or 200 °C) and after 30 min annealing at 120, 160 or 200 °C. In the last case, the X-ray measurements were taken at 30 °C after slow cooling.

It can be deduced from Fig. 6(a) that at 120 °C ECI, α and γ-crystallinities are similar to those of the initial sample, the concentration of the γ-phase being 30% and that of α-18%. After 30 min annealing at this temperature, followed by slow cooling a slight growth of 7–8% of the α-form is observed leading to the same increase in ECI. This increase is rather to be attributed to crystallization of amorphous material during the slow cooling to 30 °C and not to a phase-to-phase transition since the percentage of the γ-crystallites remains constant.

At 160 °C (Fig. 6(b)), the α-crystallinity grows, which is accompanied by a decrease of the γ-form concentration, with ECI remaining constant. Evidently, at this temperature there starts already the γ to α-phase transition, not accompanied by additional crystallization. WAXS traces at 30 °C after annealing at 160 °C, however, show an increase in both α-crystallinity and ECI, whereas the concentration of the γ-PA6 form remains almost unchanged as compared to that at 160 °C. Hence, it may be concluded that crystallization has only occurred during the slow cooling to 30 °C.

Increasing the annealing temperature of the PA6 cable to 200 °C (Fig. 6(c)) results in energetic transformation of γ into α-crystallites. Additional crystallization process takes also place at 200 °C. Obviously, these two processes continue during the slow cooling since the measurement at 30 °C reveals almost three times less γ-PA6 form as compared to its initial concentration.

Summarizing about the two polymorphic forms, annealing of oriented PA6 cable with an initial ratio of γ:α = 1.8:1.0 leads to an increase of the α-type crystallinity. Up to 120 °C, this growth is due to crystallization of amorphous material into α-PA6 form, which takes place only during the cooling. In the temperature range from 160 to 200 °C, two processes contribute to the growth of α-form: (i) crystallization of amorphous material forming α-crystals and (ii) a γ to α-form transition, the latter being better expressed above 160 °C.

Fig. 7 depicts the temperature dependence of L_B for PA6 cable annealed at various temperatures. Evidently, heating for 30 min at 120, 160 and 200 °C results in a clear increase of the long spacing, whereby the higher the temperature of annealing, the larger the increase. Upon cooling from the respective temperature to 30 °C, the trend is the same. This

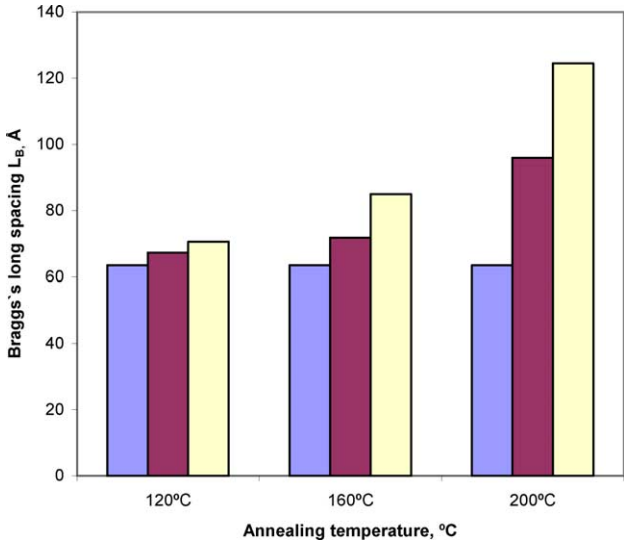

Fig. 7. Bragg's long spacing L_B in PA6 cable as a function of annealing temperature: ■ at 30 °C, initial cable before annealing; ■ in the corresponding temperature; ■ at 30 °C after 30 min annealing at the corresponding temperature.

increase of L_B can be ascribed to the above-mentioned γ to α-transition, i.e. from morphology with extended parallel PA6 macromolecules (characteristic to the γ-form) to morphologies with folded chains with anti-parallel orientation of the segments, typical of the α-form of PA6.

Fig. 8 reveals the impact of annealing temperature on the d_{hkl} spacings of α and γ-form crystalline planes in samples of differently annealed PA6 oriented cable irradiated at 30 °C. It may be concluded that annealing at 120 and 160 °C does not lead to well-expressed changes in the d_{hkl}-spacings, except for the *b*-axis of the γ-form ([γ020] plane), which grows with almost 9% even after annealing at 120 °C. The other unit cell edges suffer noticeable alteration (between 3 and 6%) only after treatment at 200 °C. These changes are different for the particular crystalline planes of the two forms. The d-spacings of the plane of H-bonded sheets, which are [002/202] for the α and [200] for the γ-form show a trend towards decrease, whereas the d-spacings of the plane of van der Waals forces between the sheets of the two crystalline forms (α[200] and γ[001] planes) tend to increase. Hence, annealing at 200 °C with a subsequent cooling to 30 °C leads to the formation of PA6 crystallites, in which the distance between the macromolecules within the sheet is larger and the inter-sheet distance is shorter than in the sample without annealing or in those annealed at lower temperatures.

5. Conclusions

1. Solid state ^{13}C NMR and WAXS studies revealed that in all four samples, irrespective of their mechanical and thermal histories, there is a co-existence of α and γ-crystalline modifications of PA6. The α-form always demonstrates a monoclinic lattice with two crystalline reflections, whereas the type of the γ-form lattice depends on the thermal conditions at which it was created and can be hexagonal (with one) or non-hexagonal (with two reflections).
2. Heating of PA6 above 120 °C always results in phase-to-phase transitions. These depend not only on the temperature (as repeatedly reported before), but also on the relative concentrations of the α and γ-crystalline forms in the starting sample. Between 120 and 160 °C, a transition from the major to the minor crystalline phase takes place (for isotropic samples it is α to γ, and for the oriented cable from γ to α-form) until reaching almost the same concentrations of the two forms. In the 160–200 °C range and especially close to the Brill

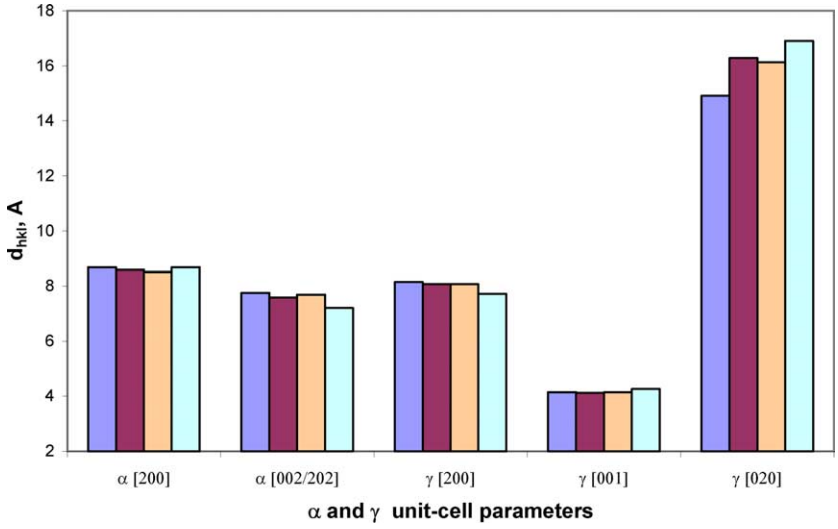

Fig. 8. Changes in α and γ-form unit cell parameters as a function of annealing temperature of oriented PA6 cable: ■ no annealing; ■ after annealing at 120 °C; ■ after annealing at 160 °C; ■ after annealing at 200 °C. All measurements are taken at 30 °C.

temperature, γ to α-transition always occurs, irrespective of all other factors.

3. Heating above 120 °C is related to L_B increase (in isotropic samples, owing to a growth of both l_c and l_a), as well as to changes in the unit cell parameters of the two crystalline forms, being the strongest at the highest temperature.
4. Quenching after melting always leads to PA6 crystallites predominantly in α-form, whereby the small amounts of remaining γ-form is with hexagonal lattice. Generally, the size of the resulting crystallites is smaller with decreased linear crystallinity x_{cl}.
5. Annealing of oriented PA6 cable at 120, 160 and 200 °C always results in an increase of the α-form content, even if the temperature is relatively low. This process is accompanied by a growth of L_B. Below the Brill transition, annealing does not change significantly the unit cell sizes of the two crystalline forms.

Acknowledgements

This work was supported by the European Community-Research Infrastructure Action under the FP6 "Structuring the European Research Area" Programme (through the Integrated Infrastructure Initiative) "Intigrating Activity on Synchrotron and Free Electron Laser Science" and HASYLAB Project II-01-006 EC. N.D. thanks for the financial support of her PhD research by grant No SFRH/BD/13435/2003 awarded by *Fundação para a Ciência e Tecnologia*, Portugal.

References

[1] Paul DR, Barlow JW, Keskkuhula H. Polymer blends. Encyclopedia of polymer science. vol. 12. New York: Wiley; 1985 pp. 399.
[2] Utracki LA. Polymer alloys and blends—state of the art. Polymer networks and blends. vol. 1 1989. pp. 61–9.
[3] Liang BR, White JL, Spruiell JE, Goswami BC. J Appl Polym Sci 1983;28(6):2011–32.
[4] Utracki LA, Dumoulin MM, Toma P. Polym Eng Sci 1986;26(1): 34–44.
[5] la Mantia FP, Valenza A. Eur Polym J 1989;25(6):553–6.
[6] Serpe G, Jarrin J, Dawans F. Polym Eng Sci 1990;30(9):553–65.
[7] Ide F, Hasegawa A. J Appl Polym Sci 1974;18(4):963–74.
[8] Chen CC, Fontan E, Min K, White JL. Polym Eng Sci 1988;28(2): 69–80.
[9] Hobbs SY, Bopp RC, Watkins VH. Polym Eng Sci 1983;23(7):380–9.
[10] Willis JM, Favis BD. Polym Eng Sci 1988;28(21):1416–26.
[11] Koulouri EG, Georgaki AX, Kallitsis JK. Polymer 1997;38(16): 4185–92.
[12] Holsti-Miettinen RM, Perttilä KP, Seppälä JV, Heino MT. J Appl Polym Sci 1995;58(9):1551–60.
[13] Evstatiev M, Fakirov S. Polymer 1992;33(4):877–80.
[14] Evstatiev M, Fakirov S, Schultz JM. Polymer 1993;34(22):4669–79.
[15] Denchev Z, Evstatiev M, Fakirov S, Friedrich K, Pollio M. Adv Compos Mater (Japan) 1998;7(4):313–24.
[16] Fakirov S, Evstatiev M, Friedrich K. From polymer blends to microfibrillar reinforced composites. In: Paul DR, Bucknall CB, editors. Polymer blends. Performance, vol. 2. New York: John Wiley; 2000. p. 455.
[17] Evstatiev M, Fakirov S, Friedrich K. Microfibrillar reinforced composites—another approach to polymer blends processing. In: Cunha AM, Fakirov S, editors. Structure development during polymer processing. Dordecht: Kluwer Academic; 2000. p. 311–25.
[18] Lin XD, Cheung WL. J Appl Polym Sci 2003;88(14):3100–9.
[19] Li ZM, Wei Y, Ll L-B, Xie BH, Huang R, Yang MB. J Polym Sci: Part B: Polym Phys 2004;42(3):374–85.
[20] Li ZM, Li L-B, Shen K-Z, Wei Y, Huang R, Yang M-B. Macromol Rapid Commun 2004;25(4):553–8.
[21] Fakirov S, Samokovliyski O, Stribeck N, Apostolov AA, Denchev Z, Sapoundjieva D, Evstatiev M, Meyer A, Stamm M. Macromolecules 2001;34(10):3314–7.
[22] Denchev Z, Oliveira MJ, Carneiro OS. J Macromol Sci Part B-Phys 2004;B43(1):143–62.
[23] Denchev Z, Oliveira MJ, Mano JF, Viana JC, Funari SSJ. Macromol Sci Part B-Phys 2004;B43(1):163–76.
[24] Varlot LK, Reynaud E, Kloppfer MH, Vigier G, Varlet JJ. Polym Sci Part B: Polym Phys 2001;39(12):1360–70.
[25] Lin L, Argon AS. Macromolecules 1992;25(15):4011–24.
[26] Fornes TD, Paul DR. Polymer 2003;44(14):3945–61.
[27] Samon JM, Schultz JM, Hsiao BS. Polymer 2000;41(6):2169–82.
[28] Gurato G, Fichera A, Grandi FZ, Zannetti R, Canal P. Makromol Chem 1974;175(3):953–75.
[29] Kyotani M, Mitsuhashi S. J Polym Sci Part A-2 1972;10(8):1497–508.
[30] Brill RZ. Phys Chem B 1943;53:61–74.
[31] Murthy NS, Aharoni SM, Szollosi AB. J Polym Sci Polym Phys Ed 1985;23(12):2549–65.
[32] Murthy NS, Curran SA, Aharoni SM, Minor H. Macromolecules 1991;24(11):3215–20.
[33] Ramesh C, Gowd EB. Macromolecules 2001;34(10):3308–13.
[34] Lincoln DM, Vaia RA, Wang ZG, Hsiao BS, Krishnamoorti R. Polymer 2001;42(25):9975–85.
[35] Salem DR, Moore RAF, Weigmann HD. J Polym Sci Part B: Polym Phys 1987;25(3):567–89.
[36] Campoy I, Gomez MA, Marco C. Polymer 1998;39(25):6279–88.
[37] Okada A, Kawasumi M, Tajima I, Kurauchi T, Kamigaito O. J Appl Polym Sci 1989;37(5):1363–71.
[38] Murthy NS. Polym Commun 1991;32(10):301–5.
[39] Murthy NS, Bray RG, Correale ST, Moore RAF. Polymer 1995; 36(20):3863–73.
[40] Murthy NS, Bednarczyk C, Moore RAF, Grubb DT. J Polym Sci Polym Phys 1996;34(5):821–35.
[41] Rhee S, White JL. Polymer 2002;43(22):5903–14.
[42] Kortleve G, Vonk CG. Kolloid-Z 1968;225:124–31.
[43] Strobl GR, Schneider M. J Polym Sci 1980;18:1343–59.
[44] Verma R, Marand H, Hsiao B. Macromolecules 1996;29:7767–75.
[45] Santa Cruz C, Stribeck N, Zachmann HG, Baltá-Calleja FJ. Macromolecules 1991;24:5980–90.
[46] Weeding TL, Veeman WS, Gaur HA, Huysmans WGB. Macromolecules 1988;21(7):2028–32.
[47] Stribeck N, Fakirov S, Apostolov AA, Denchev Z, Gehrke R. Macromol Chem Phys 2003;204(7):1000–13.
[48] Penel-Pierron L, Depecker C, Séguéla R, Lefebvre J-M. J Polym Sci Polym Phys 2001;39(5):484–95.
[49] Alexander LE. X-ray diffraction methods in polymer science. New York: Robert E. Krieger; 1979. pp. 342.